

# An Understanding of the Electrogenerated Bulk Electrolyte Species in Sodium-containing Ionic Liquid Electrolytes during the Oxygen Reduction Reaction

Cristina Pozo-Gonzalo <sup>\*a</sup>, Lee R. Johnson<sup>b</sup>, Erlendur Jónsson<sup>a</sup>, Conrad Holc<sup>b</sup>, Robert Kerr<sup>a</sup>, Douglas R. MacFarlane<sup>c</sup>, Peter G. Bruce<sup>b</sup>, Patrick C. Howlett<sup>a</sup>, Maria Forsyth<sup>a</sup>

<sup>a</sup> ARC Centre of Excellence for Electromaterials Science, Deakin University, Melbourne, Australia, Institute for Frontier Materials.

<sup>b</sup> Department of Materials, University of Oxford, Parks Road, Oxford OX1 3PH, U.K.

<sup>c</sup> ARC Centre of Excellence for Electromaterials Science, Monash University, Clayton, Victoria 3800, Australia.

Corresponding author email: [cpg@deakin.edu.au](mailto:cpg@deakin.edu.au)

## ABSTRACT

An understanding of the species generated in the bulk ionic liquid electrolyte in the presence of superoxide anion,  $O_2^{\bullet-}$ , is of interest due to its close relationship to the nature of the electrode reduction products. Unlike conventional organic solvents, ionic liquids are composed entirely of ions, thereby requiring an understanding of the intermediates generated in the bulk electrolyte.

The generation of a complex species,  $[O_2^{\bullet-}][C_4mpyr^+]_n [Na^+]_m$ , is envisioned in the bulk sodium cation pyrrolidinium-based ionic liquid with a composition depending on the  $Na^+$  concentration. In this work, the superoxide anion,  $O_2^{\bullet-}$ , has been considered in theoretical calculations regarding the oxygen reduction reaction in order to determine its average coordination number, and also its dynamics in these mixtures.

Most interestingly, the final reduction product can be tuned depending on the  $\text{Na}^+$  concentration, whereby a limited supply of  $\text{Na}^+$  favors the superoxide product while a sufficient excess of  $\text{Na}^+$  leads to the formation of the peroxide product. These findings have been identified using a pressure cell and corroborated by rotating ring-disk electrode measurements. Thus, the preferential generation of  $\text{Na}_2\text{O}_2$  over  $\text{NaO}_2$  could drastically improve the specific energy of the Na-air battery due to a higher number of electron exchanged.

## INTRODUCTION

The global effort to transition our energy supply towards renewable sources requires new energy storage technologies to meet not only current but also future needs. Metal-air batteries are especially attractive due to their superior specific energy, which is the result of the absence of heavy transition metals in the cathode active material and the use of a high energy-density metallic anode. Among this type of technology, sodium-air or sodium-oxygen cells are attracting a great deal of attention due to their high specific energy (e.g. 1605 or 1108 Wh  $\text{kg}^{-1}$ , depending on the final discharge product)<sup>1</sup>, their low production costs and the global abundance of sodium.<sup>2</sup> The first rechargeable Na-air battery was recently reported using a polyethylene glycol dimethyl ether/propylene carbonate (90:10 v/v) electrolyte, which was operated at high temperatures above the melting point of sodium in order to facilitate mass transport and reduce sodium dendrite formation.<sup>3</sup>

Under ideal conditions, discharge of a Na-air battery can lead to the formation of either the superoxide ( $\text{NaO}_2$ ;  $E^0 = 2.27$  V vs  $\text{Na}^+/\text{Na}$ ), which is kinetically favored due to the transfer of only one electron, or the peroxide ( $\text{Na}_2\text{O}_2$ ;  $E^0 = 2.33$  V vs  $\text{Na}^+/\text{Na}$ ), which is thermodynamically preferred.<sup>1</sup> This picture is further complicated by differing surface energies that could make  $\text{NaO}_2$  thermodynamically preferred at the nanoscale.<sup>4</sup>

The discharge mechanism of the Na-air battery is still under debate, particularly over the nature of the final product that is formed;  $\text{NaO}_2$ ,  $\text{Na}_2\text{O}_2$ ,  $\text{Na}_2\text{O}_2 \cdot \text{H}_2\text{O}$ ,  $\text{NaOH}$  or  $\text{Na}_2\text{CO}_3$ .<sup>5-7</sup> The nature of the discharge products and the mechanism also depends on the presence of impurities such as trace water and  $\text{CO}_2$ ,<sup>8</sup> atmosphere of operation (air vs. pure oxygen), and cathode structure and chemistry. It is also well known that the solvent and salt have a critical impact on the behavior of advanced multiphase batteries such as metal-air<sup>9 10</sup> and metal-S.<sup>11 12</sup>

The choice of organic solvent in Na-air batteries is limited due to the reactivity and poor performance of metallic Na with organic solvents, and further limited by the need for stability versus reduced  $\text{O}_2$  species. For example, carbonate-based sodium electrolytes may be relatively stable towards metallic sodium, but form  $\text{CO}_2$ ,  $\text{Na}_2\text{CO}_3$  and  $\text{NaOCO-R}$ <sup>13</sup> due to nucleophilic attack by superoxide and subsequent generation of carbonate derivatives.<sup>14</sup> Other common solvents such as DMSO are unstable when in contact with metallic Na.<sup>15</sup> In contrast, ether-based electrolytes are more stable towards electrogenerated oxygen species and metallic Na, but leave limited scope for optimization of electrolyte properties and performance.<sup>16 17</sup>

It would clearly be advantageous to optimize the Na-air battery chemistry by varying the electrolyte, however there is insufficient scope to do this using aprotic organic liquids. Ionic liquids are able to uniquely address this problem, as large variations in anion-cation composition allow for a myriad of candidate solvents. The use of ionic liquids as the electrolyte in a metal-air cell would also present other advantages such as a superior electrochemical stability allowing for a wider operational potential range, and a greater thermal stability enhancing the overall safety of the battery.<sup>18</sup> IL electrolytes have been researched to a greater extent in the case of the lithium analogue – Li-air. For example, a Li-air battery using a 0.2 M LiTFSI in  $[\text{C}_4\text{mpyr}][\text{TFSI}]$  electrolyte has been fully characterized and reportedly shows a relatively low ORR overpotential of between 0.5-0.6 V due to a smaller lithium peroxide particle size, which is the result of the slow diffusion of  $\text{Li}^+$  in the electrolyte.<sup>19</sup> Fundamental studies regarding the role of  $\text{Li}^+$  in the ORR mechanism have been

reported for imidazolium and pyrrolidinium-based ionic liquids focusing on the nature of the electrode substrate as well as the IL cation.<sup>20-21</sup> Na-air batteries using ionic liquid as electrolyte, a rechargeable Na-air battery using NaTfO/[C<sub>4</sub>mpyr][TFSI] as the electrolyte at 100 °C, has been described; however, the work focused on the composition of the solid electrolyte interphase (SEI) layer on the Na electrode surface.<sup>22</sup> These promising contributions demonstrate to the potential of ILs to overcome the challenges within the Na-air battery.

However, there are few reports regarding the influence of Na<sup>+</sup> on the oxygen reduction reaction in ionic liquids which is essential in order to understand the performance of a Na-air battery. Zhao *et al*<sup>23</sup> studied a 0.25 M NaTfO/piperidinium-based ionic liquid electrolyte and measured an ORR overpotential of 0.24 V with the discharge products claimed as NaO<sub>2</sub> and NaOH.

Of all the ionic liquids studied more broadly in relation to the ORR reaction, aliphatic and alicyclic ammonium-based ILs are known to stabilize the superoxide anion, thereby making them good candidates as electrolytes for metal-air batteries. The mechanism of the ORR in neat *N*-butyl-*N*-methylpyrrolidinium bis(trifluoromethylsulfonyl)imide ([C<sub>4</sub>mpyr][TFSI]) has been studied in detail and the process assigned to the one-electron reversible O<sub>2</sub>/O<sub>2</sub><sup>•-</sup> redox couple.<sup>24</sup> Moreover, Mohd Noor and coworkers<sup>25</sup> have reported the plating and stripping of sodium in [C<sub>4</sub>mpyr][TFSI] containing 0.5 M NaTFSI.

Recently, we reported for the first time, an extensive study on the oxygen reduction mechanism in a ([C<sub>4</sub>mpyr][TFSI]) -based ionic liquid in the presence of different Na<sup>+</sup> ion concentrations using glassy carbon as the working electrode.<sup>26</sup> The ORR showed reversible reduction processes for all concentrations, from 0.7 to 16.6 mol% NaTFSI in [C<sub>4</sub>mpyr][TFSI]. Additionally, upon increasing the Na<sup>+</sup> salt concentration, the oxygen reduction/oxidation process becomes more efficient and the onset potential of the emerging reduction process shifts to more positive values due to a superior solvation of the superoxide anion by Na<sup>+</sup>.

Subsequently, Azaceta et al.<sup>27</sup> produced a study on the electrochemical reduction of oxygen in ([C<sub>4</sub>mpyr][TFSI]) containing different metal cations including Na<sup>+</sup>. This work showed key differences in electrochemical behavior to a previous report<sup>24</sup>, which could be related to the nature of the working electrode (fluorine doped tin oxide and carbon fibers).

In this work, the use of a carbon fiber working electrode in the ionic liquid gave rise to a reversible O<sub>2</sub>/O<sub>2</sub><sup>•-</sup> redox process. However, the presence of Na<sup>+</sup> led to a negative shift in the onset of the reduction peak. This finding is not what would be expected when comparing the charge density of Na<sup>+</sup> to that of [C<sub>4</sub>mpyr]<sup>+</sup> (and therefore the acidity of the cations), and indeed differs to what has been shown previously for other systems.<sup>28</sup>

The mechanism of discharge products forming either through solution or surface precipitation has been recently studied in glyme-based systems.<sup>29</sup> Unlike glymes, ionic liquids are composed entirely of ions, thereby requiring a further understanding on the intermediates generated in the bulk electrolyte at different NaTFSI concentrations. Here, a particular emphasis will also be given to clarifying the role of the electrogenerated intermediates in the deposition product/morphology of the cathode.

To further our understanding on this topic, we also employ computational techniques focused on modelling the bulk electrolyte in order to identify the ion pairs and aggregates composed of [C<sub>4</sub>mpyr]<sup>+</sup>, [TFSI]<sup>-</sup> and Na<sup>+</sup> together with the superoxide anion, O<sub>2</sub><sup>•-</sup>. Finally, the average CN of superoxide in [C<sub>4</sub>mpyr][TFSI] has also been probed, for the first time, using molecular dynamics simulations both in the absence and presence of NaTFSI at various concentrations.

These findings are in good agreement with the electrochemistry and have proven to be a valuable tool in assigning the nature of the redox processes.

Electrochemical analysis showed that the ORR discharge mechanism occurs via a surface mechanism with predominantly thin film formation of sodium oxides. The product is confirmed to be Na<sub>2</sub>O<sub>2</sub> from

measurements of  $e^-/O_2$  ratios. SEM and EDX have been used to study the morphology of the deposit and the elemental contributions exemplify the influence of  $Na^+$  concentration and applied potential on the products.

## EXPERIMENTAL

### Materials

Sodium bis(trifluoromethylsulfonyl)imide NaTFSI (Solvionic, 99.9%) and N-butyl-N-methylpyrrolidinium bis(trifluoromethylsulfonyl)imide [C<sub>4</sub>mpyr][TFSI] (Solvionic, 99.9%) were opened and stored inside the glovebox, and used as received. The water content below 50 ppm in the ionic liquid was determined by Karl-Fischer titration (Metrohm KF 831 Karl Fischer Coulometer).

### Instrumentation and Techniques

Electrochemical experiments were performed with a Biologic VMP3/Z multi-channel potentiostat using a standard 3-electrode set-up, with a Pt wire counter electrode. A Ag/AgTfO reference electrode was manufactured by immersing a Ag wire in a 5 mM AgTfO in [C<sub>4</sub>mpyr][TFSI] solution separated from the bulk solution with a porous frit. Glassy carbon (GC, 1 mm diameter, ALS Co., Ltd. Japan) was used as the working electrode. Cyclic voltammetry was performed at 100 mV s<sup>-1</sup> scan rate. The reference electrode was calibrated versus  $Fc^+/Fc^0$  ( $E_m$ : -0.32 V). All of the experiments were performed at  $20 \pm 1$  °C.

Prior to any scan, the working electrode was polished with 0.3  $\mu$ m alumina and then washed and sonicated with deionized water (Millipore SuperQ system, resistivity 18.2 M $\Omega$  cm<sup>-1</sup>). The measurements were carried out with an IR drop compensation prior to the cyclic voltammetry experiments, which compensated for approximately 85% of the total internal resistance. The ionic liquids were bubbled with oxygen which was passed through a drying column (ultrahigh purity grade, Air Liquide) for 30 min prior to performing the voltammetry measurements, and bubbled again

between scans. Control experiments were performed inside an Argon glovebox in a nominally oxygen- and moisture-free environment.

Rotating ring-disk electrode, RRDE, measurements were performed using a MSR rotator and a removable disk rotating ring-disk electrode containing a GC disk (5 mm diameter) and a platinum ring (Pine instruments). Measurements were performed in a glove box in a round bottom flask and all necks other than the neck containing the shaft were sealed. The electrode was polished as described above between measurements. The collection efficiency at the ring,  $N$ , in each experiment was determined using an ideal redox couple.

Pressure cell measurements were performed on a Swagelok-type cell incorporating a pressure sensor (Omega Engineering). Porous composite cathodes were prepared using 90 % w.t. carbon (Super P, Timcal Ltd) and 10 % w.t. PTFE (Sigma-Aldrich), cast onto a stainless steel mesh. A glass fibre filter (Whatman) was used as the separator and Na metal was used as the anode. The cell headspace was purged with  $O_2$  for 20 minutes. The cell was maintained at constant temperature, 30 °C, throughout the experiment.

Scanning electron microscopy was performed on a JSM IT 300 series microscope and energy dispersive X-ray spectroscopy with a Oxford X-Max 50 mm<sup>2</sup> EDX detector.

## **Computational methodology**

Systems with 800 ion-pairs were constructed: pure [C<sub>4</sub>mpyr][TFSI] and a series of NaTFSI concentrations in [C<sub>4</sub>mpyr][TFSI] (1.25%, 2.5%, 5%, 10%, 20%). These systems were run with and without 10 superoxide molecules (10 fewer TFSI molecules in these runs). All initial structure were generated using Packmol <sup>30</sup>.

The force-field used was the systematic OPLS-AA based force-field from Pauda and Lopes et al. <sup>31</sup>  
<sup>32</sup>. The superoxide bonding parameters were derived from experimental values and other from OPLS-AA. All are summarized in Table 1.

**Table 1.** Force field parameters of superoxide:  $\text{O}_2^{\bullet-}$ 

Atom	$\sigma(\text{nm})$	$\varepsilon(\text{kJ/mole})$	Charge( $e$ )
O	0.296	0.878640	-0.5
Bond	$r_0(\text{nm})$	$k_r(\text{kJ mole}^{-1} \text{nm}^{-2})$	
O-O	0.128	316800	

$\sigma$ - and  $\varepsilon$ - the Lennard-Jones potential parameters,  $r_0$ - bond length,  $k_r$ - bond constant.

The program used was Gromacs 5.1<sup>33</sup>. The accompanying analysis tools were used to calculate the mean squared displacement (MSD) and radial distribution functions (RDF). Initial equilibration run was a 0.1 ns NVT run with a Nosé-Hoover thermostat (relaxation time = 1.0 ps). A subsequent NPT equilibration run was 1.0 ns long, with a Parrinello-Rahman barostat (relaxation time = 1.0 ps). Production NVT runs were 2 ns. The time step was 1 fs. Selected systems had extended NVT runs of 10 ns to analyze dynamics. The diffusion coefficients were derived from fitting the mean squared displacement curves (the Einstein relation) from 1 ns to 5 ns in 250 ps increments. Each series spanned 100 points and the resulting diffusion coefficients were averaged.

## RESULTS AND DISCUSSION

### Cyclic voltammetry

The ORR was studied in the dry  $[\text{C}_4\text{mpyr}][\text{TFSI}]$  containing low and high sodium salt concentration, viz 1.13 mol % (*ca.* 0.03 mol  $\text{kg}^{-1}$ ) and 16.6 mol % (*ca.* 0.5 mol  $\text{kg}^{-1}$ ) of NaTFSI; the latter is close to the saturation point. Typical cyclic voltammograms are shown in Figure 1 and are compared to the neat ionic liquid (Figure 1a), which is also known from previous studies.<sup>26</sup>

Considering the cyclic voltammograms recorded in the oxygen saturated low  $\text{Na}^+$  concentration (1.13 mol%) system, two reduction process were observed during the cathodic scan, C1: -1.14 V and C2: -1.27 V vs.  $\text{Fc}^+/\text{Fc}^0$  and two oxidation processes upon the subsequent anodic scan, A1: -0.57 and A2: -1.14 V vs  $\text{Fc}^+/\text{Fc}^0$ . These peaks confirm that the presence of  $\text{Na}^+$  has a significant effect on the electrochemistry of the ORR.

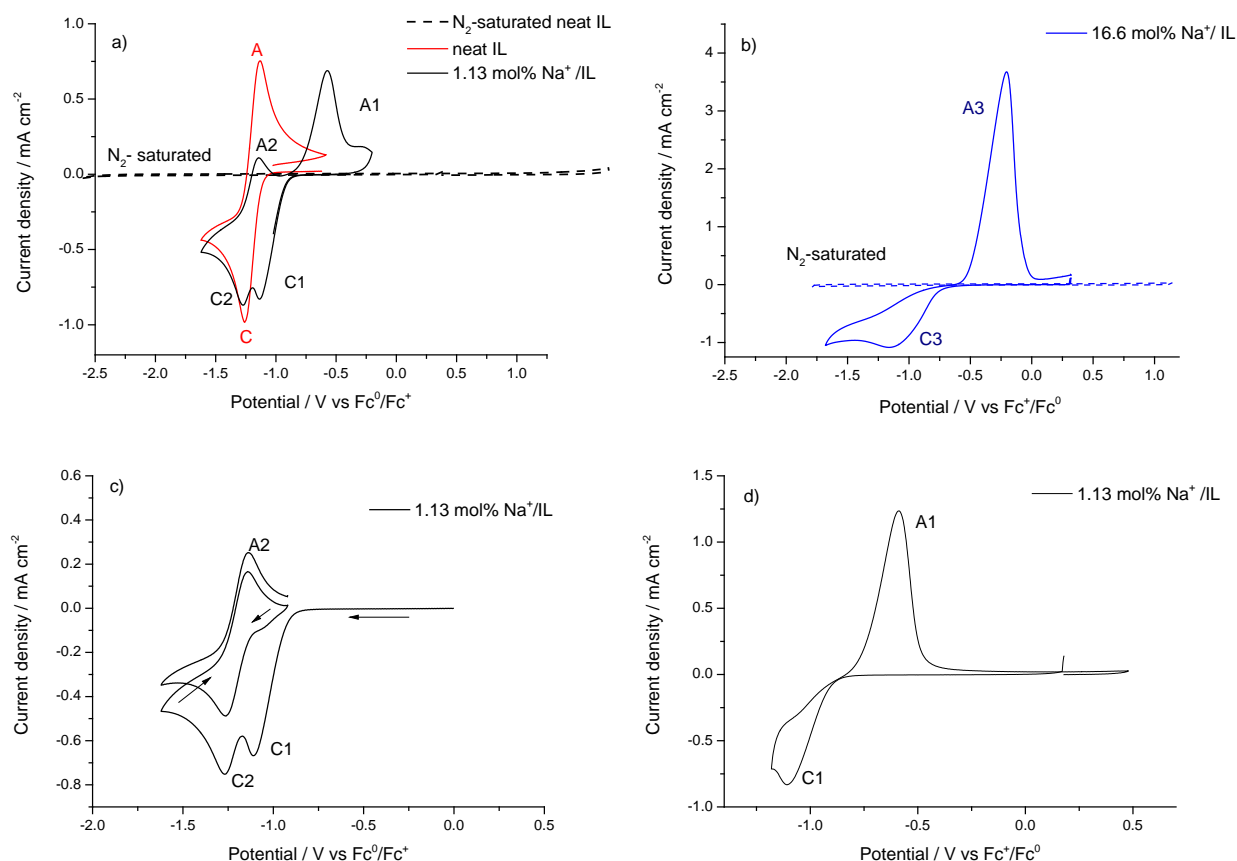
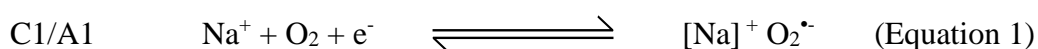


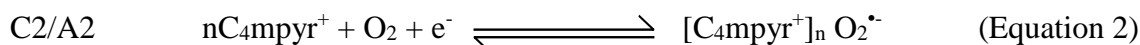
**Figure 1** Cyclic voltammograms of a glassy carbon working electrode in nitrogen saturated (dotted line) and oxygen saturated (solid line)  $[\text{C}_4\text{mpyr}][\text{TFSI}]$  containing a) 1.13 mol%  $\text{NaTFSI}$  and in neat IL and b) 16.6 mol%  $\text{NaTFSI}$ , and c, d) cyclic voltammograms of  $\text{O}_2$ -saturated  $[\text{C}_4\text{mpyr}][\text{TFSI}]$  showing different scans in the presence of 1.13 mol%  $\text{NaTFSI}$  by limiting the negative vertex at different potentials. Scan rate:  $100 \text{ mV s}^{-1}$ .

Successive scans were performed in order to identify the nature of the redox processes observed in Figure 1a. Peak A2 results from the ORR product of C2, as it is observed during cycling between -1.62 and -0.92 V vs  $\text{Fc}^+/\text{Fc}^0$  (Figure 1c). Peak A1 is the consequence of the reduction process C1 as isolated by limiting the negative vertex to -1.18 V vs  $\text{Fc}^+/\text{Fc}^0$  (i.e., before C2) upon scanning (Figure 1d).

In the neat  $[\text{C}_4\text{mpyr}][\text{TFSI}]$  (Figure 1a), the well-known one-electron  $\text{O}_2/\text{O}_2^{\bullet-}$  redox couple is seen to occur, C/A.<sup>24</sup> Upon addition of  $\text{Na}^+$  ions to this system, a C1/A1 redox couple is observed and at more positive potentials than the redox process C/A. It has been established that the  $E^0$  value of a redox process can be shifted due to changes in solvation energies.<sup>28</sup> A stronger interaction with the superoxide anion is expected in the case of  $\text{Na}^+$  cation than in the case of the pyrrolidinium cation due to a higher charge density of sodium (the ionic radius of  $\text{Na}^+$  is 0.96 Å<sup>34</sup> while  $\text{C}_4\text{mpyr}^+$  is ~ 3.30 Å<sup>35</sup>). This indicates that this new peak is due to reduction of oxygen and the formation of a Na oxide. The nature of this oxide cannot be determined from this measurement, but we consider this below in the context of further RRDE and pressure cell studies. Thus, the following mechanism for the redox couple C1/A1 is proposed;



Interestingly, the redox process C2/A2 remains upon addition of low amounts of  $\text{Na}^+$  suggesting that the one-electron  $\text{O}_2/\text{O}_2^{\bullet-}$  redox couple still occurs where the superoxide anion is coordinated by more than one cation (Equation 2).



Each of these is a variation of the main one-electron C/A process observed in the absence of Na<sup>+</sup> (Figure 1a).

The data appears to indicate that the mixtures containing low NaTFSI salt concentration allow the coordination of superoxide by two different cations (e.g. Na<sup>+</sup> and [C<sub>4</sub>mpyr]<sup>+</sup>). These findings are further corroborated by our previous study of a more diluted mixture of NaTFSI in [C<sub>4</sub>mpyr][TFSI] (*ca.* 0.7 mol% NaTFSI).<sup>26</sup> In that case, the redox process assigned to the generation of [Na]<sup>+</sup> O<sub>2</sub><sup>•-</sup> (Equation 1) appears smaller in current density and slightly more negative onset for the reduction process (*ca.* -0.94 vs -0.91 V vs Fc<sup>+</sup>/Fc<sup>0</sup>), consistent with the limiting concentration of Na<sup>+</sup> in the mixture. Theoretical calculations have been performed to elucidate the coordination of superoxide with Na<sup>+</sup> and [C<sub>4</sub>mpyr]<sup>+</sup> as a function of the Na<sup>+</sup> concentration as discussed in the following section. This is an intriguing observation as O<sub>2</sub><sup>•-</sup> is expected to favor the coordination with the harder Na<sup>+</sup> ion and undergo complete reduction at C1. We propose that the low Na<sup>+</sup> ion concentration and the sluggish diffusion of the Na<sup>+</sup> in the IL result in a depletion of Na<sup>+</sup> at the surface of the working electrode, thus allowing both reduction processes to occur, C1 and C2.

Allen et al. initiated the studies regarding the oxygen reduction mechanism in ionic liquid containing alkali salts (e.g Li<sup>+</sup>, Na<sup>+</sup>, K<sup>+</sup>). In fact, similar electrochemical behavior was reported for 0.025 M LiTFSI/[C<sub>4</sub>mpyr][TFSI] by Allen and co-workers showing also two reduction processes due to the stabilisation of superoxide by [C<sub>4</sub>mpyr]<sup>+</sup> and Li<sup>+</sup>.<sup>21</sup> However, there are differences in their electrochemistry due to the nature of the alkali metal cation. For instance, the peak potential separation is greater for the lithium metal cation with  $\Delta E_p \sim 1$  V for 0.025 M LiTFSI/[C<sub>4</sub>mpyr][TFSI] and  $\Delta E_p \sim 0.6$  V for a Na<sup>+</sup> mixture of similar concentration (*ca.* 0.03 mol kg<sup>-1</sup> NaTFSI/[C<sub>4</sub>mpyr][TFSI]). This is due to the strong Lewis acid character of Li cation in comparison with the Na cation.<sup>36</sup> These results are, therefore, very promising in the context of rechargeable Na-air batteries as lower overpotentials can be expected. A comparison with other Na<sup>+</sup>-containing IL

mixtures from the literature is more difficult due to the small number of publications. The ORR in 0.025M NaPF<sub>6</sub>/[emim][TFSI] electrolyte led to just one cathodic process instead of the 2 processes observed here.<sup>36</sup> However, it is important to highlight the different nature of the ILs involved ([C<sub>4</sub>mpyr][TFSI] vs [emim][TFSI]), particularly the known instability of imidazolium-based ionic liquids in the presence of the superoxide anion.<sup>24</sup> More recently, similar electrolyte mixture (e.g NaTFSI/[C<sub>4</sub>mpyr][TFSI]) has been studied in the context of oxygen reduction reaction at 150°C showing very different electrochemistry. For instance, the presence of Na<sup>+</sup> led to a very negative shift in the onset of the reduction peak, instead of shifting to positive values as observed in pyrrolidinium-based ILs containing a series of alkali cations.<sup>36,26</sup>

Figure 1b depicts only one reduction and one oxidation process upon increasing the sodium concentration to 16.6 mol% NaTFSI (*ca.* 0.5 mol kg<sup>-1</sup>), namely C3 at -1.16 and A3 at -0.21V vs. Fc<sup>+</sup>/Fc<sup>0</sup>. The peak potential for C3 appears at a similar potential to C1, while the peak current density increased (*ca.* ~ -0.85 mA cm<sup>-2</sup> vs. -1.1 mA cm<sup>-2</sup>). The onset of the cathodic process is shifted 0.35 V more positive by the presence of the higher Na<sup>+</sup> concentrations compared to the neat ionic liquid, however this would be detrimental to the efficiency due to an increase in peak to peak potential separation.

### Rotating ring-disk electrode (RRDE) studies

Rotating ring-disk electrode (RRDE) voltammetry was used to discern the nature and chemistry of the sodium oxide product at low and high Na<sup>+</sup> concentration. This technique allows us to overcome mass-transport limits, identify dissolved species and, separately, characterize any solid products forming at the electrode surface. Figure 2a shows the polarization curve for ORR in the neat IL. Two important features are evident; a limiting disk current at negative potentials indicates that the electrode is not passivated during reduction, while the collection of O<sub>2</sub><sup>•-</sup> at the ring mirrors the disk, thereby demonstrating its solubility and excellent reversibility in the neat IL.

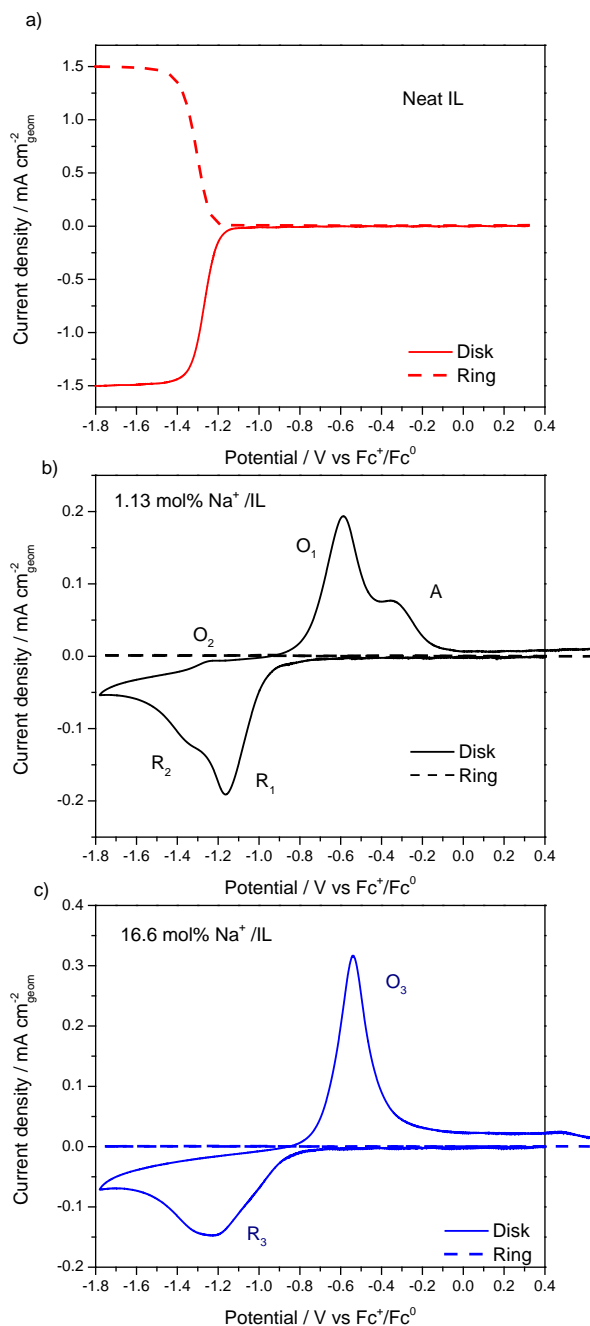


**Figure 2** Polarization curves obtained in O<sub>2</sub> saturated in a) neat [C<sub>4</sub>mpyr][TFSI], and containing b) 1.13 mol% NaTFSI and c) 16.6 mol% NaTFSI using a 5 mm diameter GC disk with a Pt ring and the rotation rate was 2000 rpm. Scan rate: 20 mV s<sup>-1</sup>

In comparison, polarisation curves in the IL containing a low Na<sup>+</sup> concentration (*ca.* 1.13 mol %) in Figure 2b displays no diffusion-limited current at the disk. Instead, two reduction peaks, namely R1 and R2, are observed. The observation of peaks in the RRDE unequivocally demonstrates the formation of a low conductivity solid which passivates the electrode. In addition, no soluble redox active species such as O<sub>2</sub><sup>•-</sup> are detected at the ring, again suggesting an insoluble solid product confined to the electrode surface.

We hypothesize that the reduction processes observed under dynamic conditions (Figure 2b) are due to the initial formation of the superoxide derivative on the electrode surface (R1) according to the mechanism described in Equation 1 and is subsequently reduced to peroxide (R2) according to Equation 3. The final discharge product is dominated by a surface mechanism that is defined by surface confined growth of Na<sub>2</sub>O<sub>2</sub>, via the intermediate NaO<sub>2</sub> <sup>29</sup>



Reversing the scan resulted in a pair of oxidation peaks consistent with formation of a surface confined thin film (Figure 2b).

The electrochemical behaviors under static (Figure 1) and dynamic conditions (Figure 2) differ due to the increased rate of supply of Na<sup>+</sup> to the working electrode in the latter case. Thus, the electroreduced oxygen species on the surface of the working electrode under dynamic conditions may coordinate preferentially to Na<sup>+</sup> as previously mentioned, at the expense of [C<sub>4</sub>mpyr<sup>+</sup>]<sub>n</sub> O<sub>2</sub><sup>•-</sup> formation. In contrast, limited Na<sup>+</sup> mass transport under static conditions forces formation of a superoxide product.

Increasing the  $\text{Na}^+$  concentration affects the shape of the  $i$ - $E$  response, resulting in a similar CV to that obtained under static conditions (Figure 1b), suggesting that at these high concentrations,  $\text{Na}^+$  is sufficiently in excess for  $\text{Na}_2\text{O}_2$  formation even under static conditions. However, the main conclusions regarding the nature of the discharge products remain the same, with additional characterization required to identify the discharge products.

### Pressure cell

In order to confirm the formation of  $\text{Na}_2\text{O}_2$  on reduction, a pressure cell was used to monitor  $\text{O}_2$  consumption in a cell during discharge (Figure 3). The  $e^- / \text{O}_2$  ratio is determined by the products that form, with values of 1 and 2 for  $\text{NaO}_2$  and  $\text{Na}_2\text{O}_2$ , respectively. An  $e^- / \text{O}_2$  ratio of 1.89 was obtained in a cell containing 1.13 mol% NaTFSI in  $[\text{C}_4\text{mpyr}][\text{TFSI}]$ .

**Figure 3** Pressure response during discharge of a Na-air pressure cell using a solution of 1.13 mol% NaTFSI in  $[\text{C}_4\text{mpyr}][\text{TFSI}]$  as the electrolyte. Ideal 1 and 2  $e^- / \text{O}_2$  responses are indicated by the dashed blue and green lines, respectively.

We believe that the initial  $\text{NaO}_2$  product is confined to the electrode surface, as shown in the RRDE experiments (Figure 2b), and then is further electrochemically reduced to  $\text{Na}_2\text{O}_2$ . This is in contrast to electrolytes where  $\text{NaO}_2$  has solubility and dissolves from the cathode surface.

These data indicate that  $\text{Na}_2\text{O}_2$  is the favored product during discharge. However, as shown during voltammetry under static and dynamic conditions, a limited supply of  $\text{Na}^+$  by mass transport could force a kinetically favored superoxide product such as  $\text{NaO}_2$  and  $[\text{C}_4\text{mpyr}]_n\text{-O}_2$ . This is likely at high rates when the diffusion of  $\text{Na}^+$  is unable to match the rate of oxygen reduction.

## Computational results

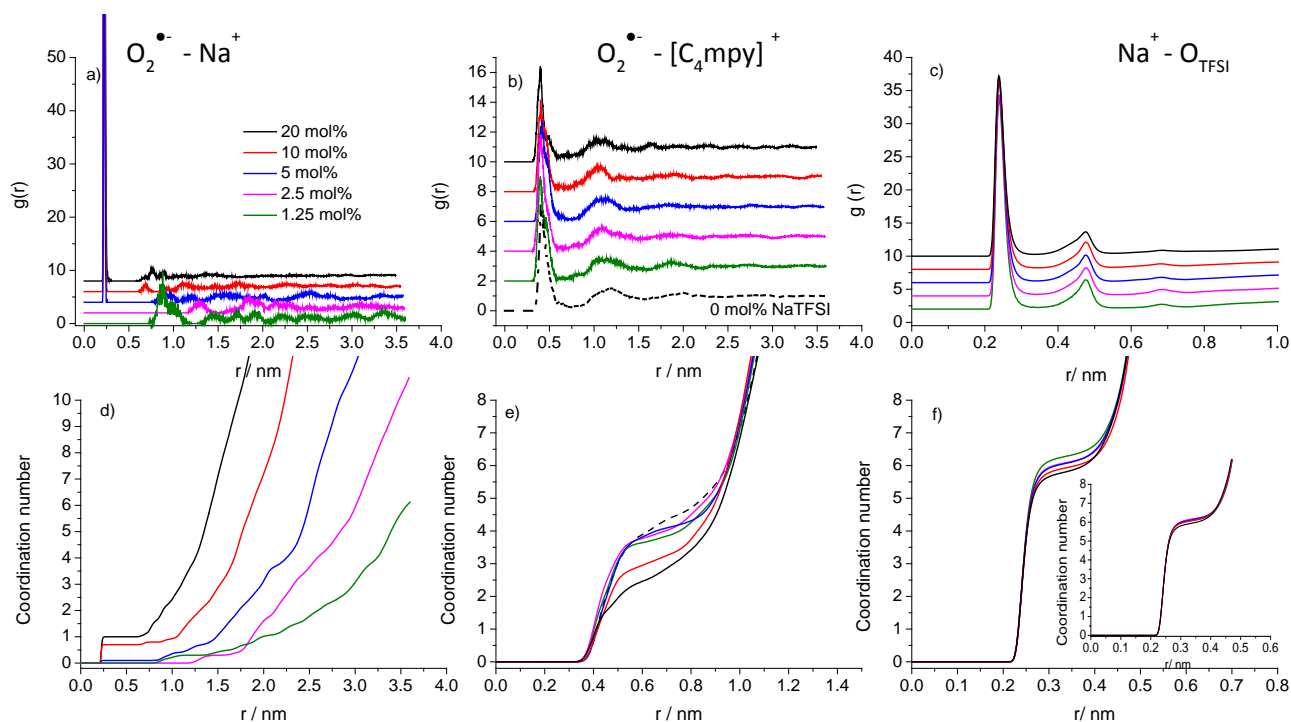


**Figure 4** Radial distribution function (RDF) of a) superoxide –  $Na^+$ , b) superoxide –  $[C_4mpyr]^+$  and c)  $Na^+ - O$  in  $[TFSI]^-$  for different sodium concentrations in  $[C_4mpyr][TFSI]$ . CN of superoxide with respect to d)  $Na^+$  and e)  $[C_4mpyr]^+$ ; and f) CN of  $Na^+$  with respect to the O in  $[TFSI]^-$  at various NaTFSI concentrations and in the presence of superoxide anions. Inset: CN of  $Na^+$  with respect to the O in  $[TFSI]^-$  as a function of NaTFSI concentration in the absence of superoxide anions.

Figure 4a and b depicts the radial distribution function (RDF) of superoxide,  $O_2^{\bullet-}$ , with respect to  $Na^+$  and  $[C_4mpyr]^+$ , respectively, at various NaTFSI concentrations ranging from 1.25 to 20 mol%. The RDF plots show the probability of  $Na^+$  and  $[C_4mpyr]^+$  to be in the proximity of the superoxide ion when the latter is located at the origin.

For the superoxide –  $Na^+$  system, the amount of superoxide molecules has been kept constant at 10, whilst the relative amount of sodium increases (starting with 10  $Na^+$  going up to 160  $Na^+$ ). The RDF of superoxide –  $Na^+$  shows that at the two lowest concentrations (1.25 and 2.5 mol%  $Na^+$ ), sodium

cations do not feature in the coordination shell of the superoxide. On the other hand, for concentrations higher than 2.5 and up to 5 mol% (20 and 40 Na<sup>+</sup>, respectively) there is a clear peak at 0.22 nm, which corresponds to the coordination of superoxide to Na<sup>+</sup> (the bond length between Na<sup>+</sup> and O<sub>2</sub><sup>•-</sup>). Moreover, the sudden appearance of this peak at 5 mol% NaTFSI implies that there is a threshold for Na<sup>+</sup>: O<sub>2</sub><sup>•-</sup> of at least 4:1 that ensures the superoxide will coordinate preferentially with Na<sup>+</sup>.

The CNs obtained from the integrated RDF can sometimes be used to reveal further details on the structural features. Closer examination of the average CN of superoxide anion with respect to Na<sup>+</sup> yields a sudden jump to a plateau and then a gradual rise with distance, both of which increase with the NaTFSI concentration (Figure 4d). Interestingly, for the 20 mol% system, a single superoxide was identified to have a CN of 3 (Figure 5b), however the values obtained for the CN in Figures 4d-f are averaged over all the molecules and also all timesteps in the simulation.

In comparison, the RDF of superoxide – [C<sub>4</sub>mpyr]<sup>+</sup> shows a similar profile in the absence and presence of NaTFSI (Figure 4b), with the coordination distance remaining unchanged at 0.4 nm. However, there is a decrease in the CN from 4 to 2 at increasing NaTFSI concentrations. This is due to the preferential coordination of superoxide to Na<sup>+</sup> over C<sub>4</sub>mpyr<sup>+</sup> lowering the relative amount of [C<sub>4</sub>mpyr]<sub>n</sub><sup>+</sup> O<sub>2</sub><sup>•-</sup> formed (process labelled as C2/A2 in Figure 1a), instead favoring the generation of [Na]<sup>+</sup> O<sub>2</sub><sup>•-</sup> (process labelled as C1/A1 process in Figure 1a), as already concluded by the cyclic voltammetry and RRDE. Thus, those findings are in good agreement with the electrochemical experiments described above.

Finally, in order to gain an understanding of the environment of  $\text{Na}^+$ , the RDF of the  $\text{Na}^+$  - O (from the  $[\text{TFSI}]^-$ ) was determined in the presence and absence of superoxide anion. As already reported in the literature by Monti et al.<sup>37</sup>,  $\text{Na}^+$  interacts with three TFSI anions to form the charge carrier  $[\text{Na}(\text{TFSI})_3]^{2-}$  in the absence of superoxide anion. In this study, the RDF of  $\text{Na}^+$  and O atoms of TFSI shows that the oxygen atoms are interacting with  $\text{Na}^+$  at a distance of 0.24 nm (seen in Figure 4c) with a similar CN to those reported in the literature. This is despite the presence of superoxide (Figure 5a), though it must be noted that our simulation methodologies do differ.<sup>37</sup>

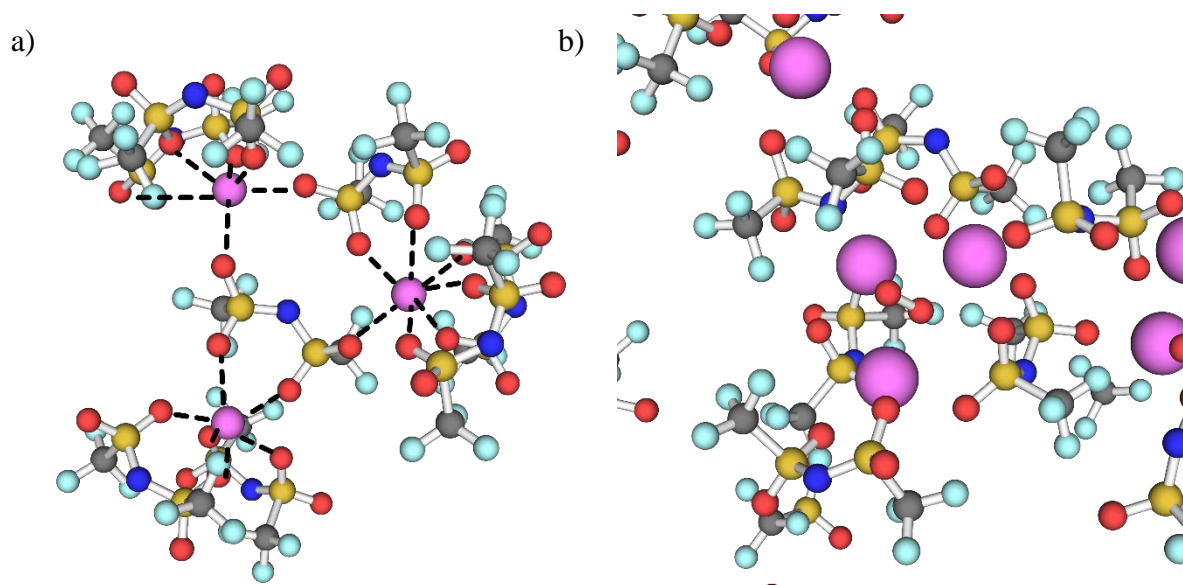


**Figure 5** a and b) Selected  $\text{Na}^+$  coordination environment in a 20 mol% NaTFSI/  $[\text{C}_4\text{mpyr}][\text{TFSI}]$  from molecular dynamics. Code used: Na: violet, N: blue, S: yellow, C: grey, F: light blue, O: red

Although superoxide does not play a significant role in the coordination distance (though it must be noted that the scarcity of superoxide will hide all but the strongest of interactions), the interaction becomes less favorable with increasing  $\text{Na}^+$  concentration and the intensity of the peak at 0.24 nm decreases, as shown by the decreasing average CN from 6 to 5 in Figure 4f.

In contrast, the average CN for Na-O<sub>TFSI</sub> remains constant as a function of NaTFSI concentration in the absence of superoxide (Figure 4f inset).

An interesting trend is observed in the dynamics of superoxide upon increasing Na<sup>+</sup> concentration in [C<sub>4</sub>mpyr][TFSI] (Figure S1). In the absence of sodium cations, the superoxide will be coordinated by four [C<sub>4</sub>mpyr]<sup>+</sup> cations. Under these conditions, the diffusion coefficient of superoxide, D(O<sub>2</sub><sup>•-</sup>) of 7.0\*10<sup>-9</sup> cm<sup>2</sup> s<sup>-1</sup> (Table 2) is in good agreement with the literature (8.6\*10<sup>-9</sup> cm<sup>2</sup> s<sup>-1</sup>).<sup>38</sup>

The dynamics of the superoxide anion, however, do slow down to one fifth in the presence of sodium cations due to the stronger interaction between the superoxide anion and Na<sup>+</sup>, which slows down the diffusion of superoxide. D(O<sub>2</sub><sup>•-</sup>) decreases dramatically when the ratio of Na<sup>+</sup> : O<sub>2</sub><sup>•-</sup> is 1:1, with a diffusion coefficient of 1.7\*10<sup>-9</sup> cm<sup>2</sup> s<sup>-1</sup>.

Interestingly, the diffusion starts increasing with the sodium concentration until reaching a similar value to that of the neat IL, (7.0\*10<sup>-9</sup> cm<sup>2</sup> s<sup>-1</sup>) in a Na<sup>+</sup>: O<sub>2</sub><sup>•-</sup> ratio of 8:1, (*ca.* 10 mol% NaTFSI). This could be related to the Na<sup>+</sup> solvation competition between superoxide anion and TFSI anion. However, the coordination of the ions in this electrolyte mixture is not that simple, and it is important to highlight that the superoxide anion will be coordinated to several cations, as established by cyclic voltammetry and corroborated by RDF. Thereby, we believe, large aggregates with a simplified formula of [O<sub>2</sub><sup>•-</sup>][C<sub>4</sub>mpyr]<sub>n</sub><sup>+</sup> [Na<sup>+</sup>]<sub>m</sub> will be generated and the composition will vary with the Na<sup>+</sup> concentration in [C<sub>4</sub>mpyr][TFSI].

There are different and opposing factors to be considered upon increasing the Na<sup>+</sup> concentration. Firstly, the number of [C<sub>4</sub>mpyr]<sup>+</sup> cations coordinated to superoxide will decrease from 4 to 2, thereby leading to a less bulky aggregate. At the same time, there is a competition between TFSI and superoxide to coordinate to Na<sup>+</sup>. A trend in the coordination has been reported for small alkali cations (M<sup>+</sup>) to sulfonylimide-based anions, whereby a greater fraction of active alkali cations is present at higher M<sup>+</sup> concentrations.<sup>39-40</sup> While the anions coordinate to the M<sup>+</sup> in a bidentate structure at low concentrations, the anions coordinate to M<sup>+</sup> in a monodentate structure in concentrated mixtures.

At concentrations close to the saturation point of NaTFSI in [C<sub>4</sub>mpyr][TFSI], the dynamics of superoxide start to decrease – probably due to less favorable physicochemical properties of the electrolyte mixtures, as already reported in the literature.<sup>25</sup> We would like to point out that, as mentioned above, the simulation data for the values of the calculated diffusivities are in good agreement with experimental data, the simulation is probing short range and short duration dynamics and so the absolute values for the mobility of D(O<sub>2</sub><sup>•-</sup>) at intermediate Na<sup>+</sup> concentrations may be overstated. With increasing Na<sup>+</sup> concentration the ion diffusivities generally decrease as the viscosity of the ionic liquid increases<sup>41</sup>, nevertheless, the trend observed here is well matched to the changes predicted by the electrochemical analyses presented previously.

**Table 2** Diffusion coefficient corresponding to superoxide anion in neat [C<sub>4</sub>mpyr][TFSI] and NaTFSI mixtures.

Electrolyte mixture	D O <sub>2</sub> <sup>•-</sup> / 10 <sup>-9</sup> cm <sup>2</sup> s <sup>-1</sup>
20 mol%	2.6
10 mol%	6.4
5 mol%	4.9
2.5 mol%	2.6
1.25 mo%	1.7
neat [C <sub>4</sub> mpyr][TFSI]	7.0

## Morphology

The morphology and elemental identification of the discharge products were studied by SEM/EDX using a glassy carbon electrode in a 3-electrode electrochemical cell held for 3 hours at potentials corresponding to the cathodic processes

At low  $\text{Na}^+$  concentration, two very different morphologies are observed depending on the reduction process under study. For instance, a patchy coating composed of platelets formed when applying a total charge of  $-0.0423 \text{ mA h cm}^{-2}$  at  $-1.05 \text{ V}$ , as shown in Figure 6a. However, deposition at a potential more negative (*ca.*  $-1.37 \text{ V}$ , Figure 6b), (total deposition charge:  $-0.38 \text{ mA h cm}^{-2}$ ) led to a more sponge-like structure. EDX analysis in both cases show a major composition of Na and O, and a small percentage of the anion of F, S and N likely corresponding to the stabilization of the superoxide by the ionic liquid or breakdown products.

Interestingly, at the higher sodium concentration a leaf-like structure is obtained with greater covering of the working electrode (total deposition charge:  $-0.163 \text{ mA h cm}^{-2}$ ) (Figure 6c). In this case, the EDX analysis shows the exclusive presence of Na and O with no breakdown products from the ionic liquid detected.

For both concentrations, the remaining bare surface of the electrodes were also analyzed by EDX showing only C and O contributions, demonstrating a successful washing of the ionic liquid mixture from the surface. Unfortunately, the geometry of the working electrode prevented the use of more accurate techniques to identify the nature of the discharge product.

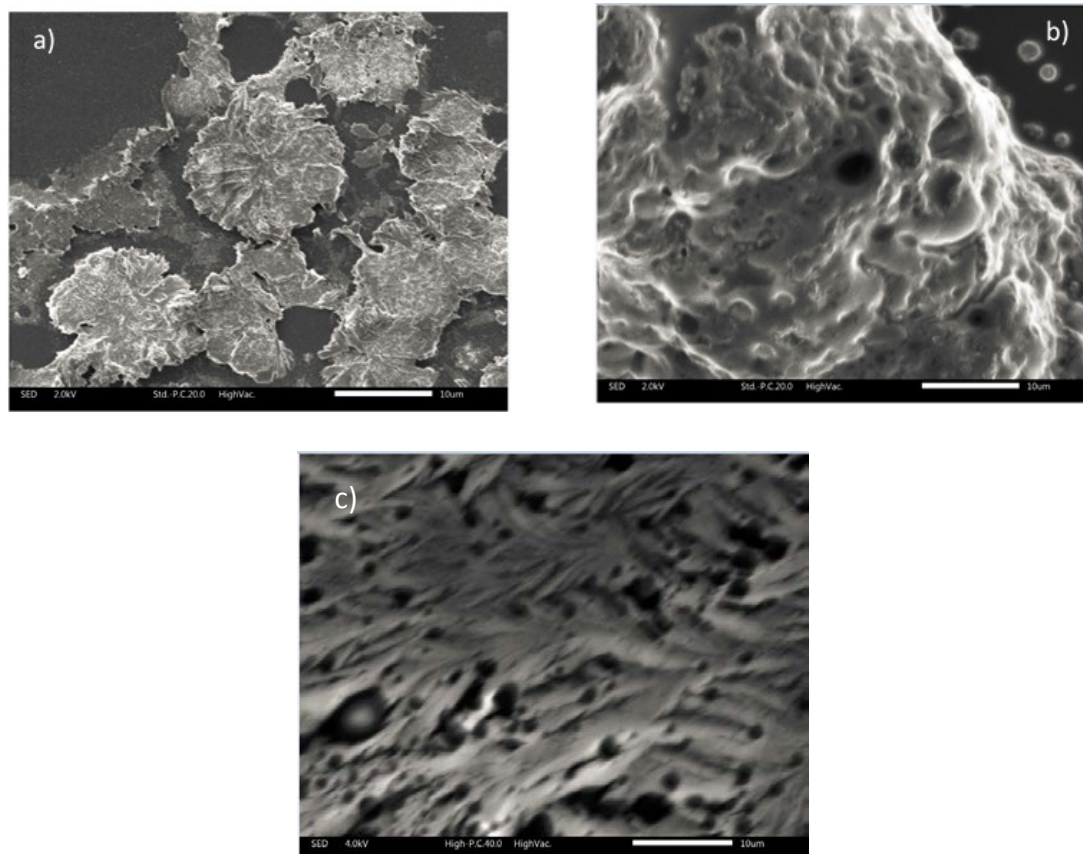


**Figure 6** SEM micrographs of a glassy carbon electrode held for 3 hours in [C<sub>4</sub>mpyr][TFSI] at constant potentials corresponding to a) -1.05, and b) -1.37 V vs Fc<sup>+</sup>/Fc<sup>0</sup> with 1.13 mol% NaTFSI, and c) -1 V vs Fc<sup>+</sup>/Fc<sup>0</sup> with 16.6 mol% NaTFSI.

## Cycling studies

Previous studies on similar system, NaFSI/[C<sub>3</sub>mpyr][FSI], showed that high sodium transference numbers and efficient Na<sup>+</sup>/Na electrochemistry could be obtained in a highly sodium concentration.<sup>39</sup> Therefore, the charge and discharge related to the oxygen reduction and evolution reactions were studied for the higher concentration electrolyte (16.6 mol% NaTFSI). The cyclability of the oxygen reduction and evolution using a GC working electrode was examined by applying a current density of  $\pm 0.1 \text{ mA cm}^{-2}$  for 10 cycles (Figure 7). The cut-off potentials were implemented to avoid degradation of the IL and irreversible side reactions involving the electrogenerated oxygen species

(i.e. to between -1.5 V and +0.1 V vs  $\text{Fc}^+/\text{Fc}^0$ ). Average values of 1.0 and 1.3  $\mu\text{Ah cm}^{-2}$  for charge and discharge capacity, respectively was attained under those working conditions with an average and constant poor efficiency of 76%, in good agreement with that obtained by cyclic voltammetry (Figure 1b). A control experiment was also performed under nitrogen to confirm the charge and discharge process as oxygen reduction and evolution.

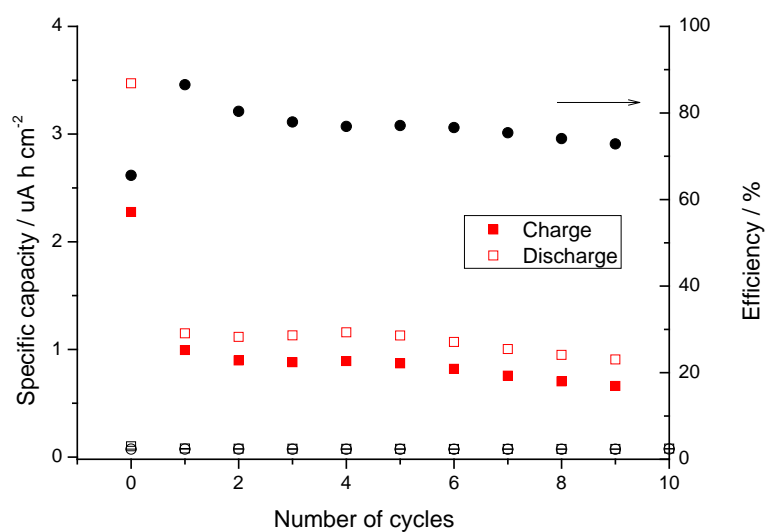


**Figure 7** Specific capacity for the charge (■) and discharge (□) processes and efficiency (●) for the  $\text{O}_2$ -saturated mixture 16.6 mol% NaTFSI / $[\text{C}_4\text{mpyr}][\text{TFSI}]$  using GC as working electrode. Applied currents  $\pm 0.1 \text{ mA cm}^{-2}$ . Potentials were limited between -1.5 V and +0.1V vs  $\text{Fc}^+/\text{Fc}^0$ . Control experiment for the  $\text{N}_2$ -saturated mixture 16.6 mol% NaTFSI / $[\text{C}_4\text{mpyr}][\text{TFSI}]$  under the same conditions discharge (◻) and charge (◉).

## CONCLUSIONS

The influence of NaTFSI concentration on the ORR mechanism in [C<sub>4</sub>mpyr][TFSI] has been studied in detail using experimental and theoretical calculations. In the absence of NaTFSI, the reduction of oxygen involves the exchange of 1 electron and the stabilization of the electrogenerated superoxide by 4 different [C<sub>4</sub>mpyr]<sup>+</sup> ions. At low Na<sup>+</sup> concentrations (*ca.* 1.13 mol%), superoxide is stabilized by both Na<sup>+</sup> and [C<sub>4</sub>mpyr]<sup>+</sup>. However, by increasing the Na<sup>+</sup> concentration the superoxide is preferentially coordinated by the sodium cation and is less available to coordinate with [C<sub>4</sub>mpyr]<sup>+</sup>.

Additionally, it is important to understand the interaction between Na<sup>+</sup> and [TFSI]<sup>-</sup> upon increasing Na<sup>+</sup> due to its role in the stabilization of superoxide, and subsequently in the deposition mechanism of the discharge products. Electrolytes containing Na<sup>+</sup> sufficiently in excess resulted in the formation of the ORR product Na<sub>2</sub>O<sub>2</sub>, via NaO<sub>2</sub>, both of which are confirmed to be insoluble. These findings have been corroborated by voltammetry, RRDE, pressure cell, and theoretical calculations.

These results highlight the opportunities that ionic liquids-based electrolytes could present when applied to Na-air devices, the most notable of which is a drastic improvement to specific energy.

Optimising the ionic liquid composition could lead to capacities and rates that exceed those obtained using organic electrolytes due to the generation of Na<sub>2</sub>O<sub>2</sub> as the final product, as opposed to NaO<sub>2</sub> that is commonly obtained in conventional organic electrolytes.

## Acknowledgements

CPG, PCH, MF, EJ and DRM gratefully acknowledge the financial support from the Australian Research Council (ARC) through the ARC Centre of Excellence for Electromaterials Science (ACES). MF and DRM also gratefully acknowledge funding through the ARC Laureate program. PGB is indebted to the EPSRC and the RCUK Energy programme including SUPERGEN for

financial support. This research was undertaken with the assistance of resources from the National Computational Infrastructure (NCI), which is supported by the Australian Government.

## References

1. Hartmann, P.; Bender, C. L.; Vračar, M.; Dürr, A. K.; Garsuch, A.; Janek, J.; Adelhelm, P., A Rechargeable Room-Temperature Sodium Superoxide (NaO<sub>2</sub>) Battery. *Nat Mater* **2013**, *12*, 228-232.
2. Ha, S.; Kim, J. K.; Choi, A.; Kim, Y.; Lee, K. T., Sodium-Metal Halide and Sodium-Air Batteries. *Chemphyschem* **2014**, *15*, 1971-1982.
3. Peled, E.; Golodnitsky, D.; Mazor, H.; Goor, M.; Avshalomov, S., Parameter Analysis of a Practical Lithium- and Sodium-Air Electric Vehicle Battery. *Journal of Power Sources* **2011**, *196*, 6835-6840.
4. Kang, S.; Mo, Y.; Ong, S. P.; Ceder, G., Nanoscale Stabilization of Sodium Oxides: Implications for Na-O<sub>2</sub> Batteries. *Nano Letters* **2014**, *14*, 1016-1020.
5. Zhao, N.; Li, C.; Guo, X., Long-Life Na-O<sub>2</sub> Batteries with High Energy Efficiency Enabled by Electrochemically Splitting NaO<sub>2</sub> at a Low Overpotential. *Phys Chem Chem Phys* **2014**, *16*, 15646-15652.
6. Bender, C. L.; Schroder, D.; Pinedo, R.; Adelhelm, P.; Janek, J., One- or Two-Electron Transfer? The Ambiguous Nature of the Discharge Products in Sodium-Oxygen Batteries. *Angewandte Chemie* **2016**, *55*, 4640-9.
7. Yadegari, H.; Sun, Q.; Sun, X., Sodium-Oxygen Batteries: A Comparative Review from Chemical and Electrochemical Fundamentals to Future Perspective. *Advanced materials* **2016**, *28*, 7065-93.
8. Xia, C.; Black, R.; Fernandes, R.; Adams, B.; Nazar, L. F., The Critical Role of Phase-Transfer Catalysis in Aprotic Sodium Oxygen Batteries. *Nature chemistry* **2015**, *7*, 496-501.
9. Johnson, L.; Li, C.; Liu, Z.; Chen, Y.; Freunberger, S. A.; Ashok, P. C.; Praveen, B. B.; Dholakia, K.; Tarascon, J.-M.; Bruce, P. G., The Role of LiO<sub>2</sub> Solubility in O<sub>2</sub> Reduction in Aprotic Solvents and Its Consequences for Li-O<sub>2</sub> Batteries. *Nature chemistry* **2014**, *6*, 1091-1099.
10. Burke, C. M.; Pande, V.; Khetan, A.; Viswanathan, V.; McCloskey, B. D., Enhancing Electrochemical Intermediate Solvation through Electrolyte Anion Selection to Increase Nonaqueous Li-O<sub>2</sub> Battery Capacity. *Proceedings of the National Academy of Sciences* **2015**, *112*, 9293-9298.
11. Zhang, S.; Ueno, K.; Dokko, K.; Watanabe, M., Recent Advances in Electrolytes for Lithium-Sulfur Batteries. *Advanced Energy Materials* **2015**, *5*, 1500117-n/a.
12. Lu, Y.-C.; He, Q.; Gasteiger, H. A., Probing the Lithium-Sulfur Redox Reactions: A Rotating-Ring Disk Electrode Study. *The Journal of Physical Chemistry C* **2014**, *118*, 5733-5741.
13. Sun, Q.; Yang, Y.; Fu, Z.-W., Electrochemical Properties of Room Temperature Sodium-Air Batteries with Non-Aqueous Electrolyte. *Electrochemistry Communications* **2012**, *16*, 22-25.
14. Balaish, M.; Kraytsberg, A.; Ein-Eli, Y., A Critical Review on Lithium-Air Battery Electrolytes. *Phys Chem Chem Phys* **2014**, *16*, 2801-2822.
15. O'Connor, D. E.; Lyness, W. I., The Reaction of Sodium and Potassium with Dimethyl Sulfoxide. The Formation and Alkylation of Methanesulfenates. *The Journal of Organic Chemistry* **1965**, *30*, 1620-1623.
16. Khetan, A.; Luntz, A.; Viswanathan, V., Trade-Offs in Capacity and Rechargeability in Nonaqueous Li-O<sub>2</sub> Batteries: Solution-Driven Growth Versus Nucleophilic Stability. *The Journal of Physical Chemistry Letters* **2015**, *6*, 1254-1259.
17. Freunberger, S. A.; Chen, Y.; Peng, Z.; Griffin, J. M.; Hardwick, L. J.; Bardé, F.; Novák, P.; Bruce, P. G., Reactions in the Rechargeable Lithium-O<sub>2</sub> Battery with Alkyl Carbonate Electrolytes. *J Am Chem Soc* **2011**, *133*, 8040-8047.
18. MacFarlane, D. R.; Tachikawa, N.; Forsyth, M.; Pringle, J. M.; Howlett, P. C.; Elliott, G. D.; Davis, J. H.; Watanabe, M.; Simon, P.; Angell, C. A., Energy Applications of Ionic Liquids. *Energy & Environmental Science* **2014**, *7*, 232-250.
19. Elia, G. A., et al., An Advanced Lithium-Air Battery Exploiting an Ionic Liquid-Based Electrolyte. *Nano Letters* **2014**, *14*, 6572-6577.

20. Allen, C. J.; Mukerjee, S.; Plichta, E. J.; Hendrickson, M. A.; Abraham, K. M., Oxygen Electrode Rechargeability in an Ionic Liquid for the Li–Air Battery. *The Journal of Physical Chemistry Letters* **2011**, *2*, 2420-2424.
21. Allen, C. J.; Hwang, J.; Kautz, R.; Mukerjee, S.; Plichta, E. J.; Hendrickson, M. A.; Abraham, K. M., Oxygen Reduction Reactions in Ionic Liquids and the Formulation of a General Orr Mechanism for Li–Air Batteries. *The Journal of Physical Chemistry C* **2012**, *116*, 20755-20764.
22. Peled, E.; Golodnitsky, D.; Hadar, R.; Mazor, H.; Goor, M.; Burstein, L., Challenges and Obstacles in the Development of Sodium–Air Batteries. *Journal of Power Sources* **2013**, *244*, 771-776.
23. Zhao, N.; Guo, X., Cell Chemistry of Sodium–Oxygen Batteries with Various Nonaqueous Electrolytes. *The Journal of Physical Chemistry C* **2015**, *119*, 25319-25326.
24. Katayama, Y.; Onodera, H.; Yamagata, M.; Miura, T., Electrochemical Reduction of Oxygen in Some Hydrophobic Room-Temperature Molten Salt Systems. *J. Electrochem. Soc.* **2004**, *151*, A59-A63.
25. Mohd Noor, S. A.; Howlett, P. C.; MacFarlane, D. R.; Forsyth, M., Properties of Sodium-Based Ionic Liquid Electrolytes for Sodium Secondary Battery Applications. *Electrochimica Acta* **2013**, *114*, 766-771.
26. Pozo-Gonzalo, C.; Howlett, P. C.; MacFarlane, D. R.; Forsyth, M., Highly Reversible Oxygen to Superoxide Redox Reaction in a Sodium-Containing Ionic Liquid. *Electrochemistry Communications* **2017**, *74*, 14-18.
27. Azaceta, E., et al., Electrochemical Reduction of Oxygen in Aprotic Ionic Liquids Containing Metal Cations: A Case Study on the Na-O<sub>2</sub> System. *Chemsuschem* **2017**, *10*, 1616-1623.
28. Gupta, N.; Linschitz, H., Hydrogen-Bonding and Protonation Effects in Electrochemistry of Quinones in Aprotic Solvents. *J Am Chem Soc* **1997**, *119*, 6384-6391.
29. Lutz, L., et al., High Capacity Na–O<sub>2</sub> Batteries: Key Parameters for Solution-Mediated Discharge. *The Journal of Physical Chemistry C* **2016**, *120*, 20068-20076.
30. Martínez, L.; Andrade, R.; Birgin, E. G.; Martínez, J. M., Packmol: A Package for Building Initial Configurations for Molecular Dynamics Simulations. *Journal of Computational Chemistry* **2009**, *30*, 2157-2164.
31. Canongia Lopes, J. N.; Pádua, A. A. H., Molecular Force Field for Ionic Liquids Composed of Triflate or Bistriflylimide Anions. *The Journal of Physical Chemistry B* **2004**, *108*, 16893-16898.
32. Pádua, A. A. H.; Costa Gomes, M. F.; Canongia Lopes, J. N. A., Molecular Solutes in Ionic Liquids: A Structural Perspective. *Accounts of Chemical Research* **2007**, *40*, 1087-1096.
33. Abraham, M. J.; Murtola, T.; Schulz, R.; Páll, S.; Smith, J. C.; Hess, B.; Lindahl, E., Gromacs: High Performance Molecular Simulations through Multi-Level Parallelism from Laptops to Supercomputers. *SoftwareX* **2015**, *1–2*, 19-25.
34. Paul, R. C.; Johar, S. P.; Banait, J. S.; Narula, S. P., Transference Number and Solvation Studies in Tetramethylurea. *The Journal of Physical Chemistry* **1976**, *80*, 351-352.
35. Appetecchi, G. B.; Montanino, M.; Zane, D.; Carewska, M.; Alessandrini, F.; Passerini, S., Effect of the Alkyl Group on the Synthesis and the Electrochemical Properties of N-Alkyl-N-Methyl-Pyrrolidinium Bis(Trifluoromethanesulfonyl)Imide Ionic Liquids. *Electrochimica Acta* **2009**, *54*, 1325-1332.
36. Allen, C. J.; Hwang, J.; Kautz, R.; Mukerjee, S.; Plichta, E. J.; Hendrickson, M. A.; Abraham, K. M., Oxygen Reduction Reactions in Ionic Liquids and the Formulation of a General Orr Mechanism for Li–Air Batteries. *J. Phys. Chem. C* **2012**, *116*, 20755-20764.
37. Monti, D.; Jónsson, E.; Palacín, M. R.; Johansson, P., Ionic Liquid Based Electrolytes for Sodium-Ion Batteries: Na<sup>+</sup> Solvation and Ionic Conductivity. *Journal of Power Sources* **2014**, *245*, 630-636.
38. Katayama, Y.; Sekiguchi, K.; Yamagata, M.; Miura, T., Electrochemical Behavior of Oxygen/Superoxide Ion Couple in 1-Butyl-1-Methylpyrrolidinium Bis(Trifluoromethylsulfonyl) Imide Room-Temperature Molten Salt. *Journal of the Electrochemical Society* **2005**, *152*, E247-E250.
39. Forsyth, M.; Yoon, H.; Chen, F.; Zhu, H.; MacFarlane, D. R.; Armand, M.; Howlett, P. C., Novel Na<sup>+</sup> Ion Diffusion Mechanism in Mixed Organic–Inorganic Ionic Liquid Electrolyte Leading to High Na<sup>+</sup> Transference Number and Stable, High Rate Electrochemical Cycling of Sodium Cells. *The Journal of Physical Chemistry C* **2016**, *120*, 4276-4286.
40. Monteiro, M. J.; Bazito, F. F. C.; Siqueira, L. J. A.; Ribeiro, M. C. C.; Torresi, R. M., Transport Coefficients, Raman Spectroscopy, and Computer Simulation of Lithium Salt Solutions in an Ionic Liquid. *The Journal of Physical Chemistry B* **2008**, *112*, 2102-2109.

41. Yoon, H.; Zhu, H.; Hervault, A.; Armand, M.; MacFarlane, D. R.; Forsyth, M., Physicochemical Properties of N-Propyl-N-Methylpyrrolidinium Bis(Fluorosulfonyl)Imide for Sodium Metal Battery Applications. *Phys Chem Chem Phys* **2014**, *16*, 12350-12355.

TOC graphic

